Structure determination of Tl/Ge(111)-(3 × 1) by surface x-ray diffraction



2008 J. Phys.: Condens. Matter 20 395226

(http://iopscience.iop.org/0953-8984/20/39/395226)

J. Phys.: Condens. Matter **20** (2008) 395226 (6pp) doi:10.1088/0953-8984/20/39/395226

# Structure determination of Tl/Ge(111)-(3 × 1) by surface x-ray diffraction

**Shinichiro Hatta[1,2], Ryosuke Ohtomo[1], Chihiro Kato[1], Osami Sakata[3], Hiroshi Okuyama[1] and Tetsuya Aruga[1,2]**

[1] Department of Chemistry, Graduate School of Science, Kyoto University, Kyoto 606-8502, Japan
[2] JST CREST, Saitama 332-0012, Japan
[3] Japan Synchrotron Radiation Research Institute, SPring-8, Kouto, Sayo, Hyogo 679-5198, Japan

E-mail: aruga@kuchem.kyoto-u.ac.jp

Received 23 July 2008, in final form 18 August 2008
Published 4 September 2008
Online at stacks.iop.org/JPhysCM/20/395226

**Abstract**

We have determined the structure of the Tl/Ge(111)-(3 × 1) surface by surface x-ray diffraction (SXRD). A Patterson function indicates the honeycomb-chain channel (HCC) structure, which is a common framework of alkali-metal-induced (3 × 1) surfaces on Si(111) and Ge(111). We examined the HCC models with different Tl adsorption sites of $H_3$ and $T_4$ and found significant differences in the simulated fractional-order rods. The HCC structure with Tl at $H_3$ shows good agreement with the experimental data. The optimized HCC structure for SXRD is consistent with the first-principles calculation and angle-resolved photoemission studies.

(Some figures in this article are in colour only in the electronic version)

## 1. Introduction

Large spin splitting of surface bands due to the Rashba-type spin–orbit interaction [1] on heavy-metal and heavy-metal-adsorbed surfaces has drawn increasing attention in recent years. The Rashba-type spin splitting of the order of 0.1 eV was first observed for the surface states on Au(111) by angle-resolved photoelectron spectroscopy (ARPES) [2]. Recently, the surface bands on the Bi surfaces and Pb- and Bi-adsorbed Ag surfaces are found to show much larger spin splitting (∼1 eV) [3–8]. These results indicate that the heavy-core potential of the adsorbed metal atoms is essential to such a giant spin splitting.

The Tl adsorption on Ge(111) induces two long-range-ordered structures of (1 × 1) and (3 × 1) at the coverage of 1 and 1/3 monolayer (ML), respectively [9]. Here, we define 1 ML as the atom density on the bulk-truncated Ge(111) surface. Tl is the heaviest element in the group-13 elements. We recently reported the spin splitting of surface bands on the Tl/Ge(111)-(1 × 1) surface [10]. Dynamical analysis of low-energy electron diffraction (LEED) revealed that Tl resides on the $T_4$ site of the bulk-truncated Ge(111) surface. In a first-principles band calculation with the spin–orbit interaction taken into account, a large spin splitting of ∼0.8 eV is found for the lowest unoccupied surface band. We found that the state with a larger contribution of the Tl 6p orbitals shows larger spin splitting. This study shows that a theoretical approach based on accurate atomic structure is very useful to understand the Rashba-type spin splitting in surface electronic structures.

The Tl-induced (3 × 1) surface was proposed to have the same structure as the alkali-metal-induced (3 × 1) surfaces on Si(111) and Ge(111) because of the similarity of the scanning tunneling microscopy (STM) images [9]. The metal-induced (3 × $n$) ($n$ = 1 and 2) surfaces have been studied with a great deal of interest as a template of one-dimensional structures on semiconductor surfaces for the last two decades [11–16]. These (3 × $n$) surfaces have a common atomic configuration called the honeycomb-chain channel (HCC) structure [13, 17, 18]. In the HCC structure, one-dimensional honeycomb chains of Si (Ge) atoms run along [1$\bar{1}$0] on the bulk-truncated (111) substrate, as shown in figures 1(a) and (b). The two adsorption sites, $T_4$ and $H_3$, of metal atoms are suggested. Here, these two HCC models are referred to as HCC-$T_4$ and HCC-$H_3$. In the STM observation

 

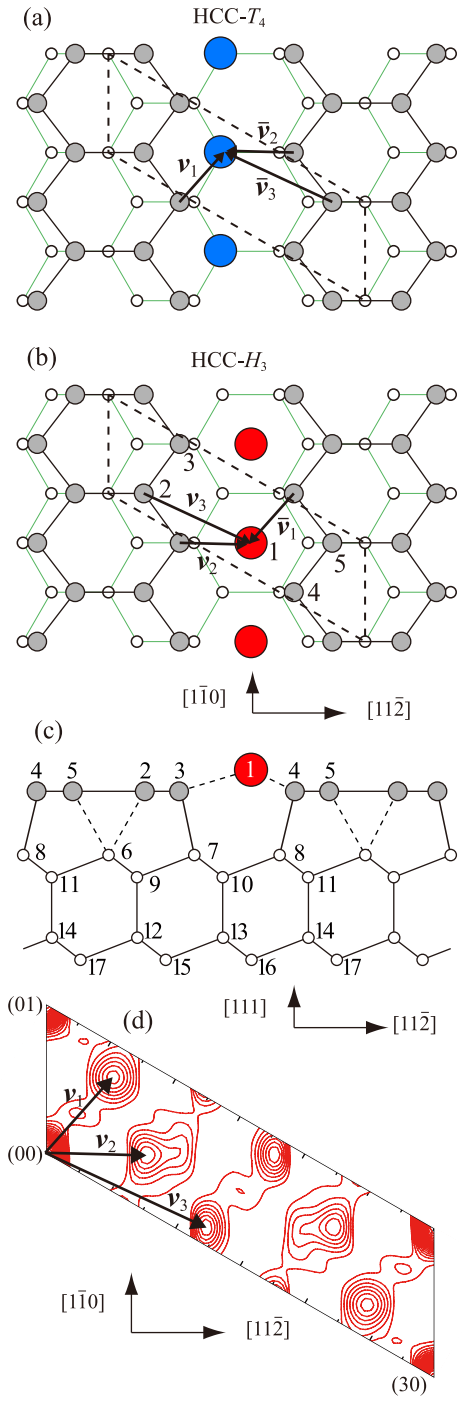


**Figure 1.** Top views of (a) the HCC-$T_4$ and (b) HCC-$H_3$ models. (c) A side view of HCC-$H_3$. Large filled circles represent Tl and small filled ones the Ge atoms of the honeycomb chain. (d) The contour map of the Patterson function obtained from in-plane fractional-order reflections at $l = 0.1$.

of Tl/Ge(111)-(3 × 1), bright zigzag chains are observed for both bias polarities [9]. Because the pattern does not show a substantial bias (polarity) dependence, the adsorption site of Tl cannot be distinguished.

The HCC structure is suggested to be stabilized by the electron donation from metal atoms and by the formation of double bonds between the inner atoms which results in the flat configuration of honeycomb chains [13]. According to the simple electron counting argument, it is found that the dangling bonds are fully terminated by one electron donation per honeycomb unit. In the case of monovalent metals, the suitable coverage is 1/3 ML. Tl generally behaves as a monovalent ions in its compounds because the 6s electron pair is quite inactive relative to the outer 6p electron. Using the first-principles calculations for HCC-$H_3$ and HCC-$T_4$ [19], we confirmed the inert-pair effect of Tl and the $\pi$ bond between the inner atoms of the honeycomb chain, irrespective of the Tl adsorption sites. While the total energy difference between HCC-$H_3$ and HCC-$T_4$ is small (∼50 meV), we found that the band structure measured by ARPES is in better agreement with the theoretical one for HCC-$H_3$. A large spin splitting up to ∼200 meV is shown in the band calculation with the spin–orbit interaction taken into account. The states with the largest spin splitting are associated with the Tl–Ge anti-bonding state and have a significant contribution of the Tl 6p orbitals as in the case of Tl/Ge(111)-(1 × 1). In order to prove the validity of these results obtained by the first-principles calculations and ARPES, the precise structure determination of Tl/Ge(111)-(3 × 1) is required.

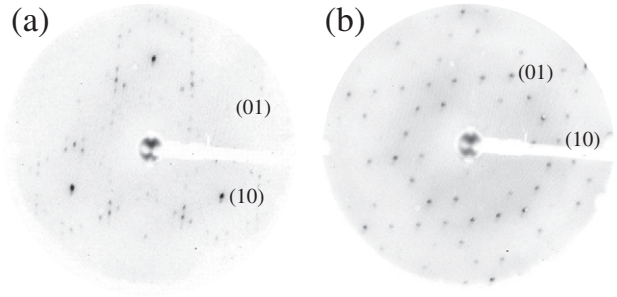


**Figure 2.** (a) Ge(111)-c(2 × 8) and (b) Tl/Ge(111)-(3 × 1) LEED patterns with 138 eV and 147 eV electrons, respectively.

In this work, we studied the atomic structure of the Tl/Ge(111)-(3 × 1) structure by surface x-ray diffraction (SXRD). We examined the HCC-$H_3$ and HCC-$T_4$ models. The HCC-$H_3$ model shows a much better agreement with the experimental data, especially for fractional-order rods, than the HCC-$T_4$ one. In the optimized HCC-$H_3$ structure, the height variation of the honeycomb-chain atoms is 0.25 Å and Tl is 0.71 Å higher than the average height of the honeycomb chain. The structure optimized for SXRD shows a qualitative agreement with that in the first-principles calculation.

## 2. Experimental details

Sample preparation and SXRD experiments were carried out using an ultra-high-vacuum (UHV) chamber mounted on a (2 + 2)-type diffractometer [20] at the beamline BL13XU of SPring-8 [21]. The Ge(111) substrate with the dimensions of 10 × 10 mm$^2$ was cut from a non-doped Ge(111) wafer (orientation accuracy $\leqslant 0.1°$). The substrate was cleaned by cycles of Ar-ion sputtering at 600 eV and annealing at 900 K by electron bombardment, until a sharp c(2 × 8) LEED pattern was observed as shown in figure 2(a). The Tl deposition of

∼1/2 ML was done by using an alumina crucible onto Ge(111) at room temperature. Subsequent annealing at 500 K for ∼1 min yielded a sharp three-domain (3 × 1) LEED pattern as shown in figure 2(b). The x-ray wavelength was set at 1.24 Å and the grazing angle at 0.5°. The measurements were done for the sample at room temperature. Diffraction intensities were recorded by $\omega$-axis scans around the surface normal. The dataset for one (3 × 1) domain consists of 374 reflections including 103 along three integer-order rods, 155 along six fractional-order rods and 116 in-plane reflections. The surface normal was aligned within less than ±0.07° to the $\omega$ axis with a laser beam. Systematic errors due to the misalignment cannot be estimated from the anisotropy of the diffraction intensity, for the HCC models are of the p1 symmetry. We assumed an error of 10% for integrated reflection intensities, in addition to the error estimated by fitting the diffraction intensities with a sum of a Lorentzian function and a slope. We used the program ANAROD to acquire structure factor amplitudes from measured scans and to perform structure refinement [22]. Here, the (3 × 1) unit cell is defined by $\boldsymbol{a}_1 = \frac{1}{2}[10\bar{1}]_{\text{cubic}}$, $\boldsymbol{a}_2 = \frac{1}{2}[\bar{1}10]_{\text{cubic}}$ and $\boldsymbol{a}_3 = [111]_{\text{cubic}}$. The in-plane reflection indices correspond to conventional LEED notation.

The density-functional-theory (DFT) calculations were performed by employing the WIEN2k computer code [23, 24]. This calculation utilizes the full-potential 'augmented plane wave + local orbitals' (APW + lo) method [25, 26] and the PBE96 generalized gradient approximation (GGA) [27] to construct the exchange and correlation potentials. We used a slab geometry consisting of Tl, the honeycomb chain and eight Ge(111) layers to simulate the Tl/Ge(111)-(3 × 1) surface (for details, see [19]).

## 3. Results and discussion

Figure 1(d) shows the contour plot of a Patterson function calculated from the structure factor amplitude of the in-plane fractional-order reflections at $l = 0.1$. Considering the inversion symmetry of the Patterson function, we found three independent peaks except for the strongest peak at each lattice point. These peaks correspond to interatomic vectors ($\boldsymbol{v}_1$, $\boldsymbol{v}_2$ and $\boldsymbol{v}_3$ in figure 1(d)) projected onto the surface plane. The peak height of the Patterson function is proportional to the product of the atomic number ($Z$) of the relevant atoms. Because $Z = 81$ of Tl is much larger than $Z = 32$ of Ge and only one Tl atom exists in a unit cell (1/3 ML), these interatomic vectors should be related to Tl–Ge. In figures 1(a) and (b), we relate these vectors to the pair of Tl and honeycomb-chain Ge atoms. This result confirms that both HCC models are possible as the Tl/Ge(111)-(3 × 1) structure.

A structure optimization for the SXRD data is performed by using a $\chi^2$ minimization scheme. The coordinates of Tl and Ge in the honeycomb chain and the two topmost bilayers are fully optimized. The anisotropic Debye–Waller (DW) factors are adopted for the Tl and honeycomb-chain Ge atoms. For the deeper Ge atoms, the isotropic bulk DW factor of 0.63 is used. Non-structural parameters of a surface fraction and roughness factor are also optimized in the fitting procedure. The domain fraction is required to simulate the

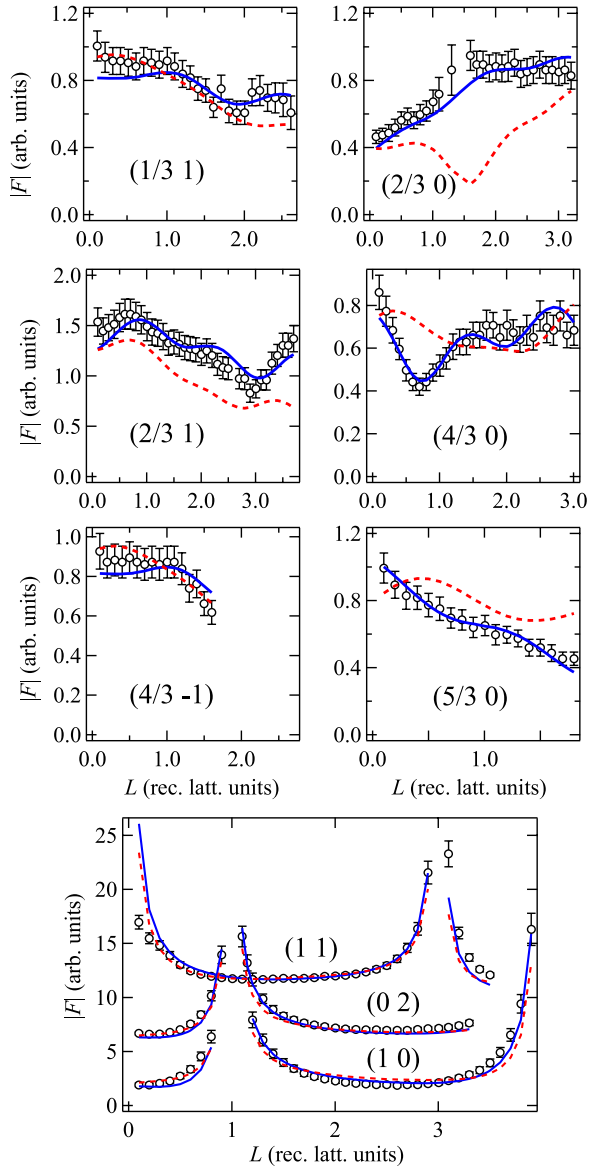


**Figure 3.** The measured structure factor amplitude (open circles) as a function of $l$ along the fractional- and integer-order rods. The solid and dashed lines represent simulated rods for HCC-$H_3$ and HCC-$T_4$, respectively. The integer-order rods of (1 1) and (0 2) are offset for clarity.

integer-order rods. Although we measured some reflections of three domains, a systematic variation is not found within error. In addition, the equivalent LEED spot intensities of three domains show no significant difference. We therefore assumed an equal fraction of the three domains. From the full width of a fractional-order spot profile at half-maximum intensity, the mean domain size was evaluated to be at least ∼250 Å.

Using only the in-plane fractional-order reflections, we obtained small $\chi^2$ values of 2.3 for HCC-$H_3$ and 4.5 for HCC-$T_4$, as expected in the Patterson function analysis. Figure 3 shows fractional- and integer-order rods. As to the integer-order rods, the simulated structure factor amplitudes for HCC-$H_3$ and HCC-$T_4$ show little difference, as shown in the bottom panel of figure 3. Somewhat featureless $l$ dependence between the bulk Bragg peaks is partially due to the small surface

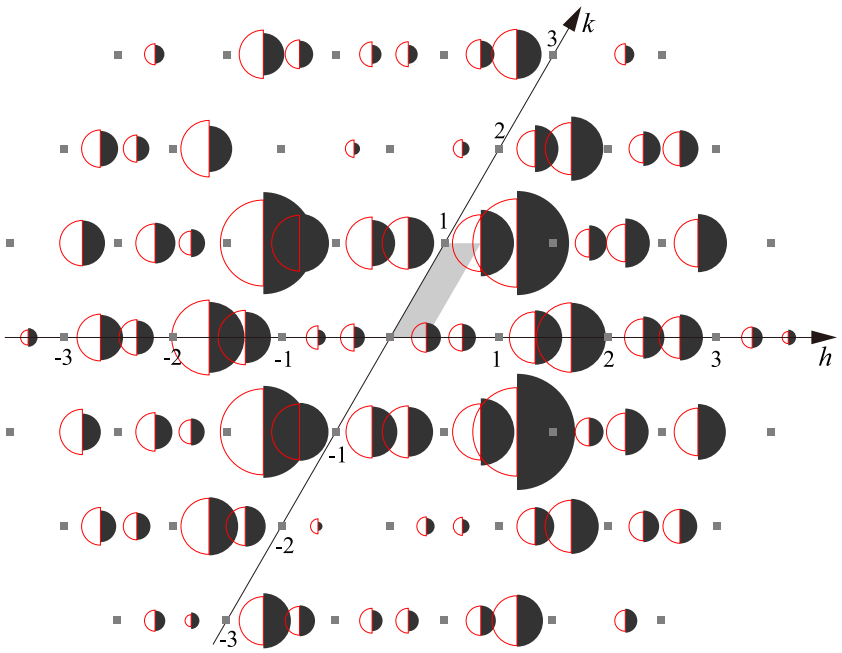


**Figure 4.** In-plane distribution of the structure factor magnitudes at $l = 0.1$. The radii of the filled (empty) half-circles are proportional to the measured (calculated for HCC-$H_3$) magnitudes. The gray squares indicate the integer-order reflections.

fraction (∼0.6). The significant difference between HCC-$H_3$ and HCC-$T_4$ is found for the fractional-order rods. While both models appear to reproduce the experimental (1/3 1), (2/3 1) and (4/3 1) rods (left columns in figure 3), much different $l$ dependences between HCC-$H_3$ and HCC-$T_4$ are shown for the (2/3 0), (4/3 0) and (5/3 0) rods (right column). Using all the measured reflections, we obtained $\chi^2 = 2.4$ for HCC-$H_3$ and 6.3 for HCC-$T_4$. Figure 4 shows the measured and simulated structure factor amplitudes of the in-plane fractional-order reflections at $l = 0.1$, showing excellent agreement.

For the $(3 \times 1)$ surfaces induced by alkali metals, the total-energy degeneracy between HCC-$H_3$ and HCC-$T_4$ is proposed by the DFT calculations, and the coexistence of HCC-$H_3$ and HCC-$T_4$ is supported by the SXRD measurements [17]. Our first-principles calculations of Tl/Ge(111)-$(3 \times 1)$ also show only a small total-energy difference of ∼50 meV. However, as shown in figure 3, it is very unlikely that the coexistence of HCC-$H_3$ and HCC-$T_4$ improves the agreement of the measured and simulated rods. Thus, we conclude that Tl atoms occupy only the $H_3$ sites on Tl/Ge(111)-$(3 \times 1)$.

The optimized atom positions of HCC-$H_3$ are given in table 1. The atom labels of the Tl and honeycomb-chain Ge atoms correspond to those in figures 1(b) and (c). The in-plane DW factors of Tl (1) and honeycomb-chain Ge (2–5) are 1–2 times larger values than the bulk value [28]. While the out-of-plane DW factors tend to exhibit larger values than those of the in-plane ones, the minima of the residual function as a function of the out-of-plane DW factors are very shallow. Thus, we tentatively fix these values at 5 for Tl and 2 for honeycomb-chain Ge, at which the structure-sensitive features of the rods are not lost. Figure 5 shows the interatomic distances of the structures optimized by SXRD and by the DFT calculation. In order to discuss bonding states and clarify the distortion of the substrate from the bulk structure, the bulk Ge–Ge distance of 2.45 Å is indicated by a solid horizontal line.

**Table 1.** Atomic positions of the optimized HCC-$H_3$ model (norm-$\chi^2 = 2.4$).

| Atom | $x$ | $y$ | $z$ | $B_\parallel$ (Å$^2$) | $B_\perp$ (Å$^2$) |
|---|---|---|---|---|---|
| #1 Tl | 1.597 | 0.299 | 1.647 | 3.57 | 5 |
| #2 Ge | 0.334 | 0.167 | 1.586 | 1.56 | 2 |
| #3 Ge | 0.753 | 0.876 | 1.574 | 1.56 | 2 |
| #4 Ge | 2.213 | 0.106 | 1.584 | 1.56 | 2 |
| #5 Ge | 2.633 | 0.817 | 1.561 | 1.56 | 2 |
| #6 Ge | −0.003 | −0.001 | 1.330 | 0.63 | — |
| #7 Ge | 0.996 | −0.002 | 1.336 | 0.63 | — |
| #8 Ge | 2.027 | 0.013 | 1.338 | 0.63 | — |
| #9 Ge | 0.339 | 0.670 | 1.251 | 0.63 | — |
| #10 Ge | 1.357 | 0.679 | 1.259 | 0.63 | — |
| #11 Ge | 2.335 | 0.668 | 1.253 | 0.63 | — |
| #12 Ge | 0.335 | 0.668 | 0.999 | 0.63 | — |
| #13 Ge | 1.345 | 0.672 | 1.009 | 0.63 | — |
| #14 Ge | 2.326 | 0.663 | 1.001 | 0.63 | — |
| #15 Ge | 0.667 | 0.339 | 0.917 | 0.63 | — |
| #16 Ge | 1.653 | 0.326 | 0.915 | 0.63 | — |
| #17 Ge | 2.653 | 0.326 | 0.917 | 0.63 | — |

The distances of Tl–Ge(3) and Tl–Ge(4) are 3.01 and 2.99 Å, respectively. While the height of Ge(3) is lower than that of Ge(4), almost the same distances of Tl–Ge result from the lateral shift of Tl from the $H_3$ site toward Ge(3). The distances are slightly larger than the sum of the covalent radius (1.23 Å) of the Ge–Ge $sp^3$ bond and the ionic radius (1.64 Å) of $Tl^+$. Tl is 0.71 Å higher than the average height of honeycomb-chain Ge atoms. The first-principles calculation shows a higher Tl position (0.95 Å). The calculated charge density of the Tl–Ge bonding state is highly polarized to Ge(3), suggesting that the inversion of the STM image contrast may be

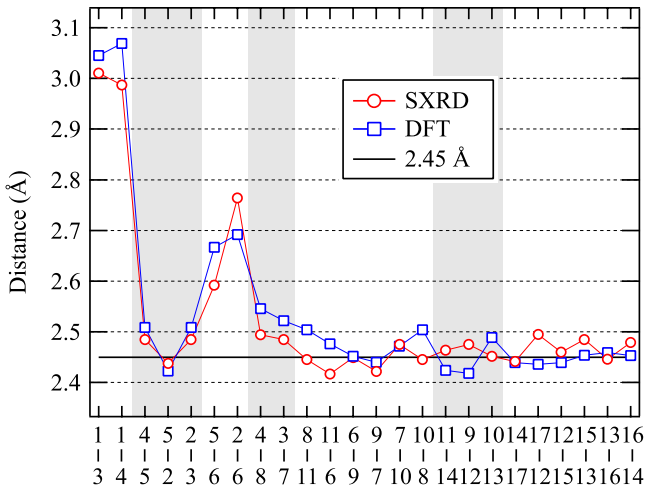


**Figure 5.** The bond lengths of HCC-$H_3$ optimized by SXRD and by the DFT calculation. The atom labels correspond to those in figure 1(c) and table 1.

observed when the bias voltage is inverted. However, because Tl is located much higher than the honeycomb chain, the Tl row is always observed as a dominant one-dimensional feature in the simulated STM images, irrespective of the polarity. This simulation is consistent with the fact that the bright rows are observed at the same position for both polarities in the experimental STM images of the Tl/Ge(111)-(3 × 1) surface [9].

The height variation in the honeycomb-chain Ge atoms are as small as 0.25 Å. The bond angles 3–2–5 and 4–5–2 are ∼125°. The flat quasi-hexagonal configuration of the Ge honeycomb chain indicates the $sp^2$-like hybridization for the inner atoms. The interatomic distance between the inner atoms (5–2) is shorter than those between the inner and outer atoms (4–5 and 2–3), as shown in figure 5. Besides, the 5–2 distances of 2.44 Å (SXRD) and 2.42 Å (DFT) are a little shorter than the bulk Ge–Ge distance of 2.45 Å. For the structures of organogermanium compounds [29], the reported bond length of Ge=Ge ranges from 2.21 to 2.51 Å and covers the value obtained by SXRD. As to the distances (5–6 and 2–6) between the honeycomb-chain inner and underlying atoms, the 5–6 distance is 0.17 Å shorter than 2–6 (a smaller difference is obtained by the DFT calculation). The existence of the double bond between the inner atoms is an important issue for comparison with the HCC structures on Si(111) [13]. Based on the fact that the Ge–Ge double bond is less stable than the Si–Si one, it was proposed for Na/Ge(111)-(3 × 1) that the double bond is absent but instead a single bond between Ge 2 (5) and 6 is formed [30]. For Tl/Ge(111)-(3 × 1), however, the 5–6 distance of 2.59 Å, as well as the 2–6 distance of 2.76 Å, is much longer than 2.45 Å, which provides no evidence for the single-bond picture. Therefore, the 2–5 bond has a stronger double-bond character than that in Na/Ge(111)-(3 × 1). This view is supported by the overall agreement between the structures optimized by SXRD and the DFT calculation [19], as shown in figure 5. The electron charge distribution of calculated states associated with the inner atoms shows $\pi$ bonding and $\pi^*$ anti-bonding characters (see figures 6(b) and (d) in [19]). Besides, the dangling bond on the substrate Ge atom (6) participates in the formation of the $\pi$ bonding state, resulting in the slight asymmetric electron charge distribution with respect to the $(1\bar{1}0)$ plane on the Ge atom (6). This is probably responsible for the small difference of the distances (5–6 and 2–6).

In the DFT calculation with the spin–orbit interaction, the large spin splitting due to the Rashba-type spin–orbit coupling is found in the unoccupied Tl–Ge (3) antibonding states having a large contribution of the Tl 6p orbital. On the other hand, because the Tl–Ge bond has an ionic character, the Tl 6p orbital has a smaller contribution to the occupied states related to the honeycomb chain, resulting in a relatively small spin splitting of at most 150 meV. The spin–orbit interaction is, therefore, expected to have only a little effect on the Tl-induced HCC structure.

## 4. Conclusions

The SXRD experiment confirmed that the Tl/Ge(111)-(3 × 1) surface has the HCC structure with the Tl adsorption site of $H_3$ (the HCC-$H_3$ structure). The geometry of the Ge honeycomb chain optimized by SXRD indicates a significant double-bond character of the bond between the inner atoms, as seen in the alkali-metal-induced (3 × 1) structures on Si(111). The SXRD result is consistent with the DFT calculation and ARPES measurements.

## Acknowledgments

The authors acknowledge the support by the Global COE Program ‘Integrated Materials Science’ (no. B-09). The synchrotron radiation experiments were performed at SPring-8 with the approval of the Japan Synchrotron Radiation Research Institute (JASRI) (proposal no. 2007A1660/BL13XU).

## References

[1] Rashba E I 1960 *Sov. Phys.—Solid State* **2** 1109
Bychkov Y A and Rashba E I 1984 *JETP Lett.* **39** 78
[2] LaShell S, McDougall B A and Jensen E 1996 *Phys. Rev. Lett.* **77** 3419
[3] Koroteev Yu M, Bihlmayer G, Gayone J E, Chulkov E V, Blügel S, Echenique P M and Hofmann Ph 2004 *Phys. Rev. Lett.* **93** 46403
[4] Hofmann Ph, Gayone J E, Bihlmayer G, Koroteev Yu M and Chulkov E V 2005 *Phys. Rev.* B **71** 195413
[5] Pacilé D, Ast C R, Papagno M, Da Silva C, Moreschini L, Falub M, Seitsonen Ari P and Grioni M 2006 *Phys. Rev.* B **73** 245429
[6] Nakagawa T, Ohgami O, Saito Y, Okuyama H, Nishijima M and Aruga T 2007 *Phys. Rev.* B **75** 155409
[7] Ast C R, Pacilé D, Falub M, Moreschini L, Papagno M, Wittich G, Wahl P, Vogelgesang R, Grioni M and Kern K 2005 arXiv:cond-mat/0509509
[8] Ast C R, Henk J, Ernst A, Moreschini L, Falub M C, Pacilé D, Bruno P, Kern K and Grioni M 2007 *Phys. Rev. Lett.* **98** 186807
[9] Castellarin-Cudia C, Surnev S, Ramsey M G and Netzer F P 2001 *Surf. Sci.* **491** 29

[10] Hatta S, Kato C, Takahashi S, Harasawa A, Okuda T, Kinoshita T, Okuyama H and Aruga T 2007 *Phys. Rev.* B **76** 075427
[11] Daimon H and Ino S 1985 *Surf. Sci.* **164** 320
[12] Fan W C and Ignatiev A 1990 *Phys. Rev.* B **41** 3592
[13] Erwin S C and Weitering H H 1998 *Phys. Rev. Lett.* **81** 2296
[14] Lee G, Hong S, Kim H, Shin D, Koo J-Y, Lee H-I and Moon D W 2001 *Phys. Rev. Lett.* **87** 056104
[15] Okuda T, Ashima H, Takeda H, An K-S, Harasawa A and Kinoshita T 2001 *Phys. Rev.* B **64** 165312
[16] Sakamoto K, Zhang H M and Uhrberg R I G 2004 *Phys. Rev.* B **69** 125321
[17] Lottermoser L, Landemark E, Smilgies D-M, Nielsen M, Feidenhansl R, Falkenberg G, Johnson R L, Gierer M, Seitsonen A P, Kleine H, Bludau H, Over H, Kim S K and Jona F 1998 *Phys. Rev. Lett.* **80** 3980
[18] Collazo-Davila C, Grozea D and Marks L D 1998 *Phys. Rev. Lett.* **80** 1678
[19] Hatta S, Kato C, Takahashi S, Harasawa A, Okuda T, Kinoshita T, Okuyama H and Aruga T 2008 *Phys. Rev.* B **77** 245436
[20] Evans-Lutterodt K W and Tang M-T 1995 *J. Appl. Crystallogr.* **28** 318
[21] Sakata O *et al* 2003 *Surf. Rev. Lett.* **10** 543
[22] Vlieg E 2000 *J. Appl. Crystallogr.* **33** 401
[23] Blaha P, Schwarz K, Madsen G K H, Kvasnicka K and Luitz J 2001 *WIEN2k, An Augmented Plane Wave + Local Orbital Program For Calculating Crystal Properties* Karlheinz Schwarz, Technical Universitat Wien, Wien, Austria
[24] Schwarz K, Blaha P and Madsen G K H 2001 *Comput. Phys. Commun.* **147** 71
[25] Sjöstedt E, Nordström L and Singh D J 2000 *Solid State Commun.* **114** 15
[26] Madsen G K H, Blaha P, Schwarz K, Sjöstedt E and Nordström L 2001 *Phys. Rev.* B **64** 195134
[27] Perdew J P, Burke K and Ernzerhof M 1996 *Phys. Rev. Lett.* **77** 3865
[28] Gao H X and Peng L-M 1999 *Acta Crystallogr.* A **55** 926
[29] Sasamori T, Sugiyama Y, Takeda N and Tokitoh N 2005 *Organometallics* **24** 3309 and references therein
[30] Lee G, Kim J, Chizhov I, Mai H and Willis R F 2000 *Phys. Rev.* B **61** 9921